

# Chapter 3

## Transition Metal-Substituted Salt of Tungsten-Based Polyoxometalate-Supported Mesoporous Silica as a Catalyst for Organic Transformation Reactions

Surjyakanta Rana and Kulamani Parida

### Contents

1	Introduction.....	58
1.1	Solid Acid Catalyst.....	58
1.2	Polyoxometalates.....	59
1.3	Heteropoly Acid.....	59
1.4	Synthesis.....	59
1.5	Structure of Heteropoly Acids.....	60
1.6	Acidic Properties of Heteropoly Acid.....	62
1.7	Redox Properties of Heteropoly Acid.....	63
1.8	Heteropoly Acid as Homogeneous Catalysis.....	63
1.9	Heteropoly Acid as Heterogeneous Catalysis.....	64
2	Experimental.....	66
2.1	Cesium Salt of Phosphotungstic Acid-Supported MCM-41 Toward Acylation of Anisole.....	66
3	Results and Discussion.....	67
3.1	Characterization.....	67
3.2	Catalytic Activity Toward Acylation of Anisole.....	68
3.3	Influence of Various Substrates.....	70
3.4	Cu Salt of Phosphotungstic Acid-Supported MCM-41 Toward Heck Vinylation Reaction.....	72
3.5	Fe-Modified Lacunary Phosphotungstate-Supported MCM-41 as an Excellent Catalyst for Acid-Catalyzed as well as Oxidation Reaction.....	76
3.6	Cs Salt of Pd Substituted Lacunary Phosphotungstate-Supported MCM-41 Toward Hydrogenation of <i>p</i> -Nitrophenol to <i>p</i> -Aminophenol.....	83
4	Conclusions.....	89
	References.....	89

---

S. Rana • K. Parida (✉)

Colloids and Materials Chemistry Department, CSIR-Institute of Minerals and Materials Technology, Bhubaneswar 751 013, Orissa, India  
e-mail: kmparida@immt.res.in

**Abstract** Solid acids and super acids are attracting substantial interest due to their applicability in many chemical industries, especially in the petroleum industry for alkylation, isomerization, and cracking reactions, as well as in the synthesis of fine chemicals. The understanding of acid-catalyzed reactions is very much important since it covers a wide field of applications, ranging from large-scale industrial processes to enzyme-controlled reactions in the living cell. This chapter deals with synthesis and characterization of different types of salts as well as transition metal-modified phosphotungstates and their applications as catalyst for acylation, Heck vinylation, bromination of phenol, oxidation of *trans*-stilbene, and hydrogenation of *ortho*-nitrophenol, respectively.

## 1 Introduction

### 1.1 Solid Acid Catalyst

A solid acid catalyst should possess high stability, numerous strong acid sites, large pores, and a hydrophobic surface providing a favorable condition for reaction and should also be economically viable. In general, a catalyst that is to be used for synthesis of biodiesel should be selective and specific and result in esterification/transesterification with high conversion and yield of biodiesel.

Traditionally almost all the chemical reactions were catalyzed by liquid acids. But, the enforcement of stringent environmental regulations has demanded the replacement of these environmentally hazardous materials, which left with no other alternative than using solid acid catalysts. More than three hundreds of solid acids have been developed in the last four decades such as natural clay minerals, cation exchange resins, zirconia, alumina, silica, mixed metal oxides, heteropoly acids (polyoxometalates), lacunary, and zeolites [1]. The surface properties and the structures have been clarified by the newly developed sophisticated analytical techniques. The characterized solid acids are applied as catalysts to various reactions, and the role of acid–base properties has been studied extensively. Now, the use of solid acid catalyst is one of the most economically and ecologically important fields in catalysis. The solid acid catalysts have many advantages over liquid Brønsted and Lewis acid catalysts such as the following: they are noncorrosive, the nature of acid sites are known, their acid strength can be modulated, and they are environmentally benign, presenting less disposal problems, and safe to handle. Their repeated use is possible and the catalyst separation from the product stream is easier. Furthermore, they can be designed and their textural properties can be engineered to develop a catalyst with higher activity, selectivity, and longer lifetime. Therefore, heterogeneous catalysis has gained so much attention and becoming more and more popular in chemical, petrochemical, and life science industries. Tanabe and Holderich [2] made a statistical survey on various types of catalysts that are used in the industrial processes. It shows that metal oxide is the second largest group of catalysts employed in industrial processes next to zeolites.

Recent report showed that heteropoly acids and heteropoly anions, like phosphotungstic acids, are efficient “super acid” catalysts which can be used both in the

homogeneous and heterogeneous phases [3]. Bulk heteropoly acids generally exhibit low catalytic performances due to their low surface areas. For this reason, the main criterion, which can lead to highly active heterogeneous acid catalysts, is an improvement of the heteropoly acid dispersion with respect to its primary acidic features. For this purpose, the main two approaches are the impregnation of the HPA on classical porous materials and the direct preparation of the acidic porous salts of HPA.

## 1.2 Polyoxometalates

Polyoxometalates (POMs) are self-assembled anionic metal oxide clusters. They are typically synthesized under acidic aqueous conditions. There are two broad classes of POMs, isopoly and heteropoly. In the heteropoly case, X is the heteroatom and is located in the center of the cluster. The element (M) that composes the framework is usually molybdenum or tungsten. The heteroatom is often P=3 or Si=4, but there are numerous examples for over 70 different elements.

## 1.3 Heteropoly Acid

Heteropoly acids (HPAs) are the acidic forms of polyoxometalates. They are widely used as homogeneous and heterogeneous acids and oxidation catalysts due to their unique physicochemical properties. Generally, all heteropoly acids are strong acids. This strong acidity can be attributed to the delocalization of surface charge density throughout the large sized polyanion, leading a weak interaction between the proton and the anion.

Solid HPAs in the acid form are more efficient catalyst than conventional solid acids. The ability to absorb large amount of polar molecules in the bulk, coupled with high proton mobility, leads to a high catalytic efficiency for liquid phase reaction. They have been widely used as acid and oxidation catalyst for organic synthesis, and they are found in several industrial applications. HPA is used as catalyst due to the following properties:

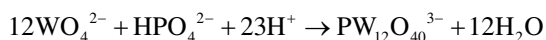
1. Solubility in aqueous and organic media
2. Intrinsic multifunctional, strong acidity (Brønsted sites), and redox properties

They are also of great interest as model systems for studying fundamental problems of catalysis.

## 1.4 Synthesis

Preparation of heteropoly acids is getting more and more importance for their applications. Such heteropoly acids as  $H_3PW_{12}O_{40}$ ,  $H_4SiW_{12}O_{40}$ , and  $H_3PMo_{12}O_{40}$

are commercially available as crystalline hydrates. The simplest way to prepare heteropoly acids involves the acidification of an aqueous solution containing the oxoanions and the heteroatom:



Control of the pH and the ratio of central atom to metal atom (X/M) is necessary to obtain the desired structure. Acidification is achieved by direct addition of a mineral acid.

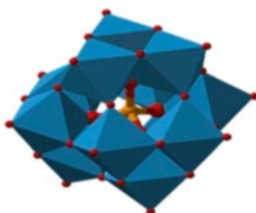
## 1.5 Structure of Heteropoly Acids

Heteropoly acids are polymeric oxoanions with well-defined primary structure. They are made by the combination of hydrogen and oxygen with certain metals and nonmetals. Various types of heteropoly acid are known each having its own characteristic structure like:

1. Keggin structure
2. Silverton structure
3. Dawson structure
4. Waugh structure
5. Anderson structure

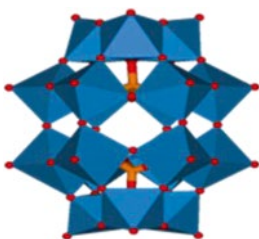
### 1.5.1 Keggin Structure

Keggin heteropoly acids have general formula  $\text{X}^{n+}\text{M}_{12}\text{O}_{40}^{n-8}$ , where X is the central atom ( $\text{Si}^{4+}$ ,  $\text{Ge}^{4+}$ ,  $\text{P}^{5+}$ ,  $\text{As}^{5+}$ , etc.),  $n$  the degree of its oxidation, and M is molybdenum or tungsten, which can be partly replaced by other metals [4]. The structure of Keggin compounds comprises four trigonal groups of edge-sharing  $\text{MO}_6$  octahedral, each group sharing corners with neighboring groups and with the central tetrahedron. In each octahedron, the metal is displaced toward the terminal oxygen atoms. This structural arrangement leads to the formation of a spherical polyanion. The first characterized well-known heteropoly compound is the one having Keggin structure which is fairly stable and easily available.



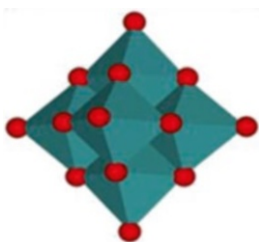
### 1.5.2 Wells–Dawson Structure

Well–Dawson structure heteropoly acids have general formula  $[X_2M_{18}O_{62}]$ , where  $X$  is  $P^{5+}$ ,  $S^{6+}$ ,  $As^{5+}$  and  $M$  may be either  $W^{6+}$  or  $Mo^{6+}$ . These HPCs are formed by dimerization of  $PM_9O_{34}$  moieties, thus under suitable conditions of pH. It consists of two half units, each of which is derived from the Keggin structure by removal of three adjacent corner linked  $MO_6$  octahedron anions, leaving three octahedra over a ring of six.



### 1.5.3 Anderson Structure

Anderson structure of heteropoly acid has general formula  $[XM_6O_{24}]$ , where  $X$  is  $Mn^{4+}$ ,  $Ni^{4+}$ ,  $Pt^{4+}$ ,  $Te^{6+}$  and  $M$  may be either  $W^{6+}$  or  $Mo^{6+}$ . The structure is planar in which each  $MoO_6$  octahedron has two terminal oxygen and the heteroatom  $X$  adopts the octahedral coordination. Anderson anions are usually obtained from aqueous solutions at a pH of 4–5.



### 1.5.4 Silverton Structure

Silverton structure of heteropoly acid has general formula  $[XM_{12}O_{42}]$ , where  $X$  is  $Ce^{4+}$ ,  $Th^{4+}$  and  $M$  may be either  $W^{6+}$  or  $Mo^{6+}$ . The central atom is surrounded by 12 oxygen atoms that form an icosahedron (12 vertices, 20 faces, and 30 sides) as a central polyhedron around which  $MO_6$  octahedra are arranged in a face sharing pairs.

### 1.5.5 Waugh Structure

Waugh structure of heteropoly acid has general formula  $[XM_9O_{32}]$ , where X is  $Mn^{4+}$ ,  $Ni^{4+}$  and M may be either  $W^{6+}$  or  $Mo^{6+}$ . It is built around an octahedral coordinated heteroatom. Three octahedral addenda atoms are arranged at the vertices of a triangle, which is coplanar with the central  $XO_6$  octahedron and another two groups of edge-shared  $M_3O_{13}$  triplets, are placed above and below the middle layer of the four octahedral.

## 1.6 Acidic Properties of Heteropoly Acid

The acid–base properties of heteropoly compounds can be modified by the choice of the hetero atom, oxometal in the primary structure, and the cation [5]. The acidity can be generated by the protons which act as counter cations in heteropoly acids (i.e., in  $H_3PMO_{12}O_{40}$ ) and in mixed acidic salts (for instance, in  $K_xH_{3-x}PW_{12}O_{40}$ ). There are two types of protons in crystalline HPA: (1) nonlocalized hydrated protons bound to one metal cation as a whole and rapidly exchanging with the protons of the water molecules in the hydration shell of the acid and (2) nonhydrated protons localized at the peripheral oxygen atoms of the polyanion [4].

All heteropoly acids are strong acids, much stronger than conventional solid acids such as  $SiO_2-Al_2O_3$ ,  $H_3PO_4/SiO_2$ , and HY and HX zeolites and mineral acids as  $H_2SO_4$ , HCl, and *p*-toluenesulfonic acid. They are completely dissociated in aqueous solutions and partly dissociated in organic solvents. This strong acidity can be attributed to the delocalization of surface charge density throughout the large sized polyanion, leading to a weak interaction between the protons and the anion. The order of acid strength is the same as that observed in solution.

The acid strength can be expressed by the Hammett acidity function  $H_0$ :  $H_0 = pK_{BH^+} - \log\left(\frac{[BH^+]}{[B]}\right)$  where [B] is the concentration of the indicator B,  $[BH^+]$  is the concentration of the conjugated acid, and  $K_{BH^+}$  is the equilibrium constant for the reaction:  $BH^+ \rightarrow B + H^+$ .

The  $[BH^+]/[B]$  ratio can be determined by spectroscopy in the UV and visible bands or can be measured more roughly by visually observing the point in the titration at which the color changes.

The  $H_0$  value of 100 %  $H_2SO_4$  (−11.94) is taken as a reference number. The acids with values >12 are classified as superacids [6]. Superacids with  $H_0$  values of −20 (i.e., 108 times stronger than 100 %  $H_2SO_4$ ), such as  $HSO_3F$  and  $SbF_5$ , are able to protonate methane.

According to this scale heteropoly compounds can be classified as super acid compounds. This extraordinarily high acidity has led to increasing interest in the possibility of using them as alternative catalysts for acid-catalyzed transformations which employ environmentally homogeneous liquid acids like HF,  $AlCl_3$ , or  $H_2SO_4$ . On the other hand, a very high acidity may be responsible for undesired side reactions and for quick deactivation phenomena due to the formation of heavy

by-products. The possible way to control the acid properties is through partial neutralization of the protons, which can be achieved by exchanging the acid form with a suitable metal ion.

### 1.7 Redox Properties of Heteropoly Acid

The redox properties of HPA are a function of the nature of the metal atoms in the primary structure (addenda atoms) and of both the heteroatom and the counterions. In solutions, the reduction potentials of heteropoly anions containing Mo and V are high as these ions are easily reduced. Oxidative ability decreases generally in the order  $V > Mo > W$  containing heteropoly anions, which means that the vanadium-containing heteropoly compounds are the strongest oxidants [7]. The replacement of one or more molybdenum atoms in the primary structure of Keggin heteropoly compound of molybdenum for vanadium leads to an enhancement of the oxidation potential of the heteropoly compound due to the vanadium reducibility.

The nature of the heteroatom affects the overall charge of the polyanion. An increase in the charge leads to a decrease in the oxidation potential for the  $W^{6+}/W^{5+}$  couple in  $P^V W_{12}O_{40} > Si^{IV} W_{12}O_{40} \approx Ge^{IV} W_{12}O_{40}^{4-} > B^{III} W_{12}O_{40}^{5-} \approx Fe^{III} W_{12}O_{40}^{5-} > H_2 W_{12}O_{40} \approx Co^{II} W_{12}O_{40}^{6-} > Cu^I W_{12}O_{40}^{7-}$ .

The effect of the counter cation may be significant. When the cation is easily reducible, the redox properties of the heteropoly compound are parallel to those of the cation. When the cation is not reducible, like alkali metals, the reducibility of the metal in the primary structure is nevertheless affected by the nature of the cation [5]. The oxidizing ability has been estimated from the rate of reduction of heteropoly compounds by  $H_2$ , CO, and organic compounds, but sometimes the data appear inconsistent, due to the difference in the kind of reductant, homogeneity, nonstoichiometry, and decomposition of the catalysts [3].

### 1.8 Heteropoly Acid as Homogeneous Catalysis

Heteropoly acids catalyze a wide variety of reactions in homogeneous liquid phase offering strong options for more efficient and cleaner processing compared to conventional mineral acids [8]. In principle, mechanisms of homogeneous catalysis by heteropoly acids and by ordinary mineral acids are of the same origin. Both HPAs and mineral acids function as proton donors [9]. There are, however, some specific features in the HPA catalysis. First, being stronger acids, HPAs have significantly higher catalytic activity than mineral acids. In organic media, the molar catalytic activity of heteropoly acid is usually 100–1,000 times higher than that of  $H_2SO_4$  [4]. This makes it possible to carry out the catalytic process at a lower catalyst concentration and/or at a lower temperature. Further, heteropoly acid catalysis lacks side reactions such as sulfonation and chlorination, which occur with mineral acids.

As stable, relatively nontoxic crystalline substances, HPAs are also preferable as regard to safety and ease of handling [8].

The relative activity of Keggin heteropoly acids depends primarily on their acid strength. Other properties such as the oxidation potential, the thermal, and hydrolytic stability are also important factors. These properties for the most common heteropoly acids are summarized below:

Acid strength:  $\text{H}_3\text{PW}_{12}\text{O}_{40} > \text{H}_4\text{SiW}_{12}\text{O}_{40} > \text{H}_3\text{PMo}_{12}\text{O}_{40} > \text{H}_4\text{SiMo}_{12}\text{O}_{40}$

Oxidation potential:  $\text{H}_3\text{PMo}_{12}\text{O}_{40} > \text{H}_4\text{SiMo}_{12}\text{O}_{40} \gg \text{H}_3\text{PW}_{12}\text{O}_{40} > \text{H}_4\text{SiW}_{12}\text{O}_{40}$

Thermal stability:  $\text{H}_3\text{PW}_{12}\text{O}_{40} > \text{H}_4\text{SiW}_{12}\text{O}_{40} > \text{H}_3\text{PMo}_{12}\text{O}_{40} > \text{H}_4\text{SiMo}_{12}\text{O}_{40}$

Hydrolytic stability:  $\text{H}_4\text{SiW}_{12}\text{O}_{40} > \text{H}_3\text{PW}_{12}\text{O}_{40} > \text{H}_4\text{SiMo}_{12}\text{O}_{40} > \text{H}_3\text{PMo}_{12}\text{O}_{40}$

Generally, tungsten heteropoly acids are the catalysts of choice because of their stronger acidity, higher thermal stability, and lower oxidation potential compared to molybdenum heteropoly acids. Usually, if the reaction rate is controlled by the catalyst acid strength,  $\text{H}_3\text{PW}_{12}\text{O}_{40}$  shows the highest catalytic activity in the Keggin series. However, in the case of less demanding reactions as well as in reactions at higher temperatures in the presence of water,  $\text{H}_4\text{SiW}_{12}\text{O}_{40}$ , having lower oxidation potential and higher hydrolytic stability, can be superior to  $\text{H}_3\text{PW}_{12}\text{O}_{40}$ . Some homogeneous reactions catalyzed by HPA are hydration of olefins, esterification reaction, condensation of acetone to mesityl oxide, and alkyl benzenes.

The major problem, limiting the utility of homogeneously catalyzed processes, is the well-known difficulty in catalyst recovery and recycling. As the cost of the heteropoly acids is higher than mineral acids, the recycling of heteropoly acid catalyst is the key issue to their application. Only a few homogeneous reactions allow for easy heteropoly acid recycling like hydration of olefins. In some cases, HPA can be recovered from polar organic solution without neutralization by precipitating with a hydrocarbon solvent. HPA can also be extracted from an acidified aqueous solution of its salt with a polar organic solvent. Even though the neutralization of HPA is necessary, the amount of alkali needed and the amount of waste formed there upon is much less than that of mineral acids. A more efficient way to overcome the separation problem is the use of biphasic systems or solid heteropoly acid catalysts [8, 9].

## 1.9 Heteropoly Acid as Heterogeneous Catalysis

Solid heteropoly acids are more efficient than conventional solid acids, like zeolites,  $\text{SiO}_2$ , and  $\text{Al}_2\text{O}_3$ , due to their ability to absorb large amount of polar molecules in the bulk, coupled with high proton mobility, which leads to a high catalytic efficiency for liquid phase reactions. This behavior favors the reaction kinetics and the participation of all structural protons in the reaction [5]. This high activity allows the operation to be carried out at milder conditions than that of other solid acids. Obvious advantage of heterogeneous systems over homogeneous is easy separation of a catalyst from reaction products. Furthermore, since heteropoly



acids are soluble only in wet polar solvents, their strong acidity cannot be utilized in homogeneous systems [8]. Therefore, heteropoly acids must be used as solid acid catalyst for catalyzing highly demanding reactions like Friedel–Crafts reaction. In order to enhance the acid strength, solid heteropoly acid catalysts are usually dehydrated by evacuating at 150–300 °C for 1–2 h [10].

A serious problem with the solid heteropoly acid catalysts is their deactivation during organic reactions due to the coke formation on the catalyst surface, which remains to be solved to put heterogeneous heteropoly acid catalysis in practice. Instead of burning the coke as in the case of alumina silicates and zeolites, supporting heteropoly acids on a carrier inhibits the formation of coke on the catalyst surface.

### 1.9.1 Supported Heteropoly Acids

The drawback of heteropoly acids is their low surface area (1–10 m<sup>2</sup>/g) that limits their application in many reactions. This disadvantage can be overcome by dispersing the heteropoly acid on solid supports with high surface area. The catalytic activity of supported heteropoly acid depends mainly on the heteropoly acid loading, the pretreatment conditions, and the type of carrier. Generally, heteropoly acids strongly interact with supports at low loading levels, while the bulk properties of heteropoly acids prevail at high loadings. Acidic or neutral substances like SiO<sub>2</sub>, active carbon, acidic ion-exchange resin, and TiO<sub>2</sub> are suitable supports, but on the other hand, solids like Al<sub>2</sub>O<sub>3</sub> and MgO having basicity tend to decompose heteropoly acids [8], causing a significant decrease in catalytic activity.

### 1.9.2 HPA on Silica

SiO<sub>2</sub> is relatively inert toward heteropoly acids above a certain loading level. The thermal stability of silica-supported heteropoly anions decreases with respect to that of the bulk acid, particularly at low concentrations. On the other hand, tungstic acid keeps its Keggin structure when impregnated on silica, provided tungsten content is greater than 10 % w/w but at lower contents the acid may experience partial degradation.

Moffat and Kasztelan [11] have concluded that the Keggin structure of phosphotungstic acid dispersed on silica is maintained even after calcination at 550 °C. At low loadings, H<sub>3</sub>PW<sub>12</sub>O<sub>40</sub> and H<sub>4</sub>SiW<sub>12</sub>O<sub>40</sub> form finely dispersed species on the surface of silica and a heteropoly acid crystal phase is developed at heteropoly acid loading above 50 wt%. Silica-supported tungsten HPAs like H<sub>3</sub>PW<sub>12</sub>O<sub>40</sub> and H<sub>4</sub>SiW<sub>12</sub>O<sub>40</sub> maintain the Keggin structure at high loadings but decompose at very low loadings because of the strong interactions with surface silanol groups.

A study based on the synthesis of chemicals catalyzed by transition metal/salts of tungsten-based polyoxometalate-modified mesoporous silica (MCM-41) in the liquid phase has been focused in this article. We will also comment

briefly on the preparation of the modified catalyst by various methods and its characterization by different techniques, as well as on the structure and the active sites. It is out of the scope of this article to cover comprehensively all reactions that have ever been reported using tungsten-based polyoxometalate-modified MCM-41-based solid acids.

## 2 Experimental

### 2.1 Cesium Salt of Phosphotungstic Acid-Supported MCM-41 Toward Acylation of Anisole

Salts of HPA were prepared by partially exchanging protons of the parent HPA with large cations, such as  $\text{Cs}^+$ ,  $\text{K}^+$ ,  $\text{Rb}^+$ , and  $\text{NH}_4^+$ , which could be water insoluble and present a rather high surface area ( $>100 \text{ m}^2/\text{g}$ ) [10, 12]. Extensive studies have been carried out over Cs salt of HPA supported on metal oxides such as  $\text{Al}_2\text{O}_3$ ,  $\text{MgO}$ , silica, titania, and zirconia, MCM-41, MCM-48, and SBA-15 [13–15]. The catalytic activities of these materials have been investigated thoroughly for various alkylation, acylation, esterification reactions, etc. [16]. Recently, the effect of acylating agent on the acylation of anisole using mesoporous silica-supported HPA and Cs salt of HPA has been studied by various research groups [17–19]. Cardoso et al. reported 90 % of conversion for acylation of anisole taking phosphotungstic acid-supported silica as catalyst [17]. Kaur and Kozhevnikov [18] reported the acylation of anisole with carboxylic acids on  $\text{Cs}_{2.5}$ -HPA as catalyst having 51 % yields. Kamala and Pandurangan reported butylation of anisole taking phosphotungstic acid-supported Al MCM-41 as catalyst [20]. Acylation of aromatic compounds is a widely used reaction for the production of fine chemicals, pharmaceutical, and cosmetics. So many papers are published in Cs salts of PTA supported on different supports, but our catalysts are different from others and characterized by different techniques and also focus on various organic transformation reactions.

#### (a) Synthesis of MCM-41

In a typical synthesis process, 1.988 g of cetyl trimethyl ammonium bromide (CTAB, 98 %, S.D. fine chem.) was dissolved in 120 g of water at room temperature. After complete dissolution, 8 ml of aqueous  $\text{NH}_3$  (32 % in water, Merck) was added to the above solution. Then 10 ml of tetraethyl orthosilicate (TEOS, 99 %, Aldrich) was added to the solution under vigorous stirring (300 rpm). The hydrolysis of TEOS takes place during the first 2 min at room temperature (the solution becomes milky and slurry forms), whereas the condensation of the mesostructured hybrid material is achieved after 1 h of reaction. The material was then filtered and allowed to dry under static air at  $80^\circ\text{C}$  for 12 h. The surfactant removed mesoporous material was obtained by acid treatment method. For acid extraction, the as-obtained materials (1 g) were treated with a mixture of ethanol (100 ml) and concentrated HCl (1 ml, 38 % in weight) at  $80^\circ\text{C}$  for 6 h.

(b) Synthesis of Cs Salt of Phosphotungstic Acid

Cs of phosphotungstic acid ( $\text{Cs}_{2.5}\text{H}_{0.5}\text{PW}_{12}\text{O}_{40}$ ) was prepared by adding the  $\text{Cs}_2\text{CO}_3$  solution dropwise to the PTA solution according to the literature method [10]. The resulting precipitate was dried at 110 °C overnight in vacuum and calcined at 300 °C for 3 h. The chemical composition of the samples was determined using ICP atomic emission spectrometer (PerkinElmer).

(c) Synthesis of Cs Salt of Phosphotungstic Acid Supported on MCM-41

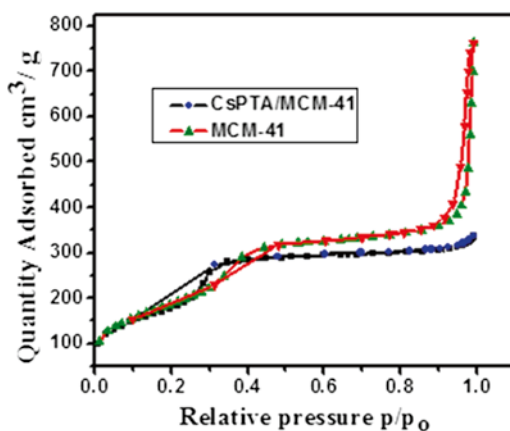
MCM-41 was first impregnated with aqueous solution of the  $\text{Cs}^+$  precursor ( $\text{Cs}_2\text{CO}_3$ ), dried at 110 °C for 12 h. Following this, a methanolic solution of PTA was impregnated, dried at 110 °C for 12 h, and calcined at 200. The catalysts are designated as  $x$  Cs-PTA/MCM-41 ( $x=10\text{--}60$  wt%).

### 3 Results and Discussion

#### 3.1 Characterization

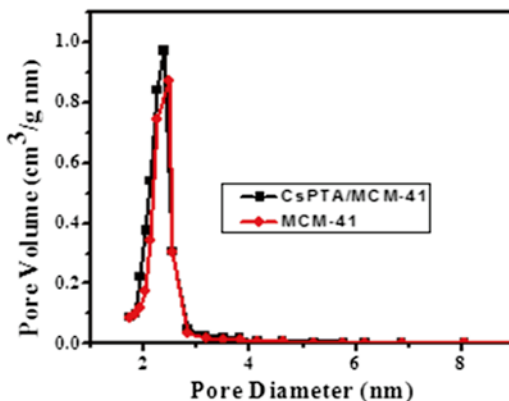
##### 3.1.1 Surface Area and Pore Size Distribution

Figure 3.1 shows the nitrogen adsorption–desorption isotherms of the parent and modified samples. MCM-41 shows a type IV isotherm with a sharp inflection capillary condensation step at  $P/P_0=0.35$ , corresponding to the pore size of about 2.7 nm. Apart from the narrow pore size distribution, MCM-41 exhibits an H1-type hysteresis loop at  $P/P_0$  between 0.9 and 1, reflecting secondary mesoporosity due to inter particle condensation [21]. In case of the modified sample, the sharp capillary condensation step shifts to low relative pressure of  $P/P_0=0.1$ , indicating the decrease in pore volume and surface area after modification. A reasonable explanation for this



**Fig. 3.1**  $\text{N}_2$  adsorption–desorption isotherms of MCM-41 and 50 wt% Cs-PTA/MCM-41

**Fig. 3.2** Pore size distribution of MCM-41 and 50 wt% Cs-PTA/MCM-41 sample



observation is that most of the Cs-PTA clusters were introduced into the pore and the partial blockage of one-dimensional mesopores of MCM-41 by small aggregates of Cs-PTA [21].

The pore size distribution curves of the samples are shown in Fig. 3.2. The pore size distribution curves show that there is slight decrease in pore diameter after impregnation of Cs salt of PTA.

### 3.1.2 FTIR Studies

The FTIR spectra of Cs-PTA and Cs-PTA loaded MCM-41 are shown in Fig. 3.3. The spectra show a broad band around 3,100–3,600  $\text{cm}^{-1}$ , which is due to adsorbed water molecules. The absorption band due to H–O–H bending vibration in water is at 1,620–1,640  $\text{cm}^{-1}$ . The absorption band around 1,087–1,092  $\text{cm}^{-1}$  is due to Si–O asymmetric stretching vibrations of Si–O–Si bridges. The characteristic signature of the Keggin structure was seen in each case, with dips at 1,080, 985, 890, and 800  $\text{cm}^{-1}$ . The band assignments are available in the literature [22, 23].

### 3.1.3 SEM Studies

SEM micrographs of Cs-PTA/MCM-41 microcrystals recorded at different magnifications are shown in Fig. 3.4a and b. Each crystal has a cylindrical form having diameter ranging from 0.4 to 0.6  $\mu\text{m}$ . The total length of the crystals is 1–2  $\mu\text{m}$  and consists of packages of cylindrical fibers (Fig. 3.4a).

## 3.2 Catalytic Activity Toward Acylation of Anisole

The acylation reaction was carried out in the liquid phase in a 50 ml three-necked round-bottom flask fitted with a thermometer, reflux condenser with  $\text{CaCl}_2$  guard tube, and a magnetic stirrer. A mixture of 100 mmol anisole and 10 mmol of acetic anhydride

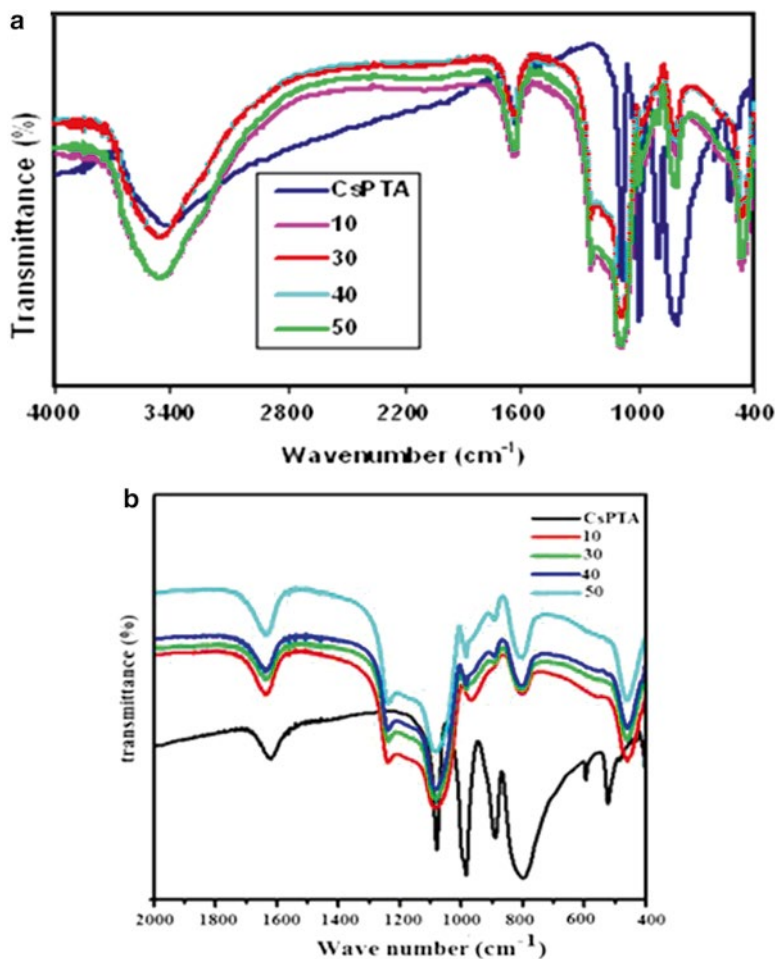
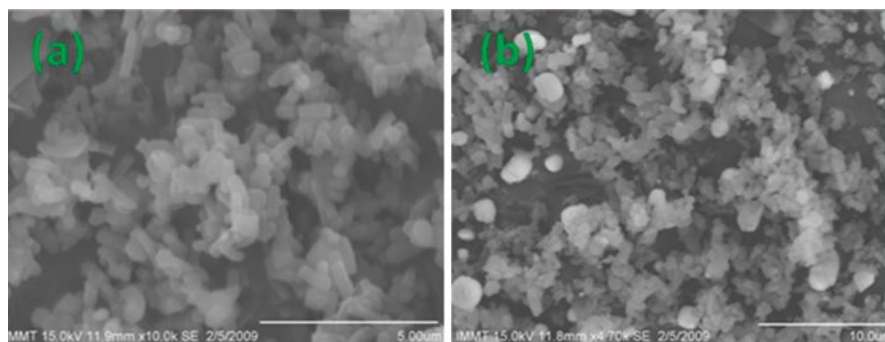


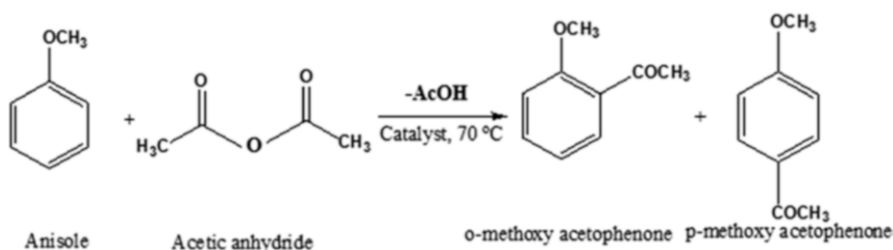
Fig. 3.3 FTIR spectra of Cs-PTA/MCM-41 samples (a) 400–4,000  $\text{cm}^{-1}$ , (b) 400–2,000  $\text{cm}^{-1}$

was added to the flask along with 0.1 g of *n*-tridecane, which was used as an internal standard for GC analysis. The catalyst was added after adjusting the temperature to 70 °C. The reaction mixture was separated from the catalyst after 1 h and analyzed by off-line gas chromatography (GC) as shown in Scheme 3.1 (Table 3.1).

Among the catalysts with different Cs-PTA loadings, the 50 wt% Cs-PTA/MCM-41 catalyst gave the highest conversion (98 %). Further, increase in the Cs-PTA loading decreases the acetic anhydride conversion. The sample containing 60 wt% Cs-PTA shows 95 % conversion. The activity of the catalysts has been found to be related to the number of Brønsted acid sites. Since no metal ion was present in the reaction filtrate, it is presumed that the true active species is the solid acid, which developed due to chemical interaction between the Cs-PTA and MCM-41. This also supports that the catalyst is stable under reaction conditions.



**Fig. 3.4** Different magnification of scanning electron micrograph of 50 wt% Cs-PTA/MCM-41



**Scheme 3.1** Schematic representation of acylation of anisole

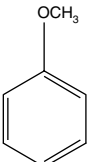
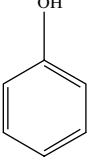
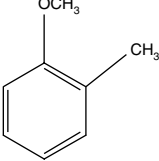
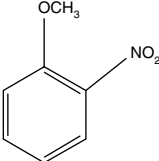
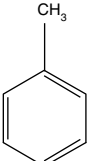
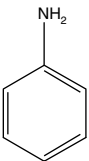
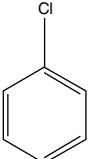
**Table 3.1** Liquid phase acylation of anisole over 50 wt. % Cs-PTA/MCM-41 and comparison of the result with other reported methods

Catalyst used	Reactant	Conversion (%)	References
Phosphotungstic acid/silica	Acetic anhydride	90	[24a]
Cs <sub>2.5</sub> H <sub>0.5</sub> PW <sub>12</sub> O <sub>40</sub>	Dodecanoic acid	51	[24b]
ZSM-5	Acetic anhydride	90	[24c]
Aluminosilicates	Octanoyl chloride	90	[24d]
Cs <sub>2.5</sub> H <sub>0.5</sub> PW <sub>12</sub> O <sub>40</sub> /silica	Acetic anhydride	50	[24e]
Cs <sub>2.5</sub> H <sub>0.5</sub> PW <sub>12</sub> O <sub>40</sub> /K-10	Benzoyl chloride	37	[24f]
H <sub>3</sub> PW <sub>6</sub> Mo <sub>6</sub> O <sub>40</sub> /Zirconia	Acetic anhydride	89	[24g]
Cs-PTA/MCM-41	Acetic anhydride	98	Our work

### 3.3 Influence of Various Substrates

The reaction procedure was applied to anisole as well as activated aromatic compounds such as toluene, aniline, and deactivated compounds such as chlorobenzene, and the results were summarized in Table 3.2. The results show that introduction of an electron withdrawing group (e.g., nitro group) on the aromatic ring substantially decreases the conversion of acylation, while an electron-donating group (e.g., CH<sub>3</sub>

**Table 3.2** Effect of substrate on acylation reaction

Substrate	Conversion (%)	Selectivity	
		Para	Ortho
	98	97	3
	94	96	4
	99	100	–
	65	100	–
	75	90	10
	90	92	8
	35	75	25

Substrate = 100 mmol, acetic anhydride = 10 mmol, catalyst amount = 0.1 g, temperature = 70 °C, time = 1 h

group) increases it. Like anisole, aniline and phenol give preferentially para product in high yield. Activated aromatic compounds such as toluene gives around 72 % conversion having 61 % of para selectivity. Chlorobenzene was sluggish in the acylation reaction and gave very low conversion.

### 3.4 *Cu Salt of Phosphotungstic Acid-Supported MCM-41 Toward Heck Vinylation Reaction*

A lot of papers have already been published on Cs, K, and Na salts of PTA toward various reactions [25a, b]. A few publications are also there on the salts of PTA supported on MCM-41 [25c]. However, there has been no example on the use of Cu salt of HPA supported on MCM-41 for the Heck vinylation of aryl halides with olefins. Hence for the first time, we have performed the coupling reaction using  $\text{Cu}_x\text{H}_{3-2x}\text{PW}_{12}\text{O}_{40}/\text{MCM-41}$  as catalyst in aqueous medium.

#### 3.4.1 Preparation of Catalyst

The Cu salt of the  $\text{H}_3\text{PW}_{12}\text{O}_{40}$  was prepared [25d] as precipitate by adding 0.18 g of  $\text{Ba}(\text{OH})_2$  (to neutralize 3 protons) to the aqueous solution containing 2 g of  $\text{H}_3\text{PW}_{12}\text{O}_{40}$ . Later 0.16 g of  $\text{CuSO}_4 \cdot 5\text{H}_2\text{O}$  was added to replace Ba with Cu by eliminating Ba as  $\text{BaSO}_4$ . The  $\text{Cu}_{1.5}\text{PW}_{12}\text{O}_{40}$  salt was recovered from the solution by recrystallization. Varying the amount of  $\text{Ba}(\text{OH})_2$  and  $\text{CuSO}_4 \cdot 5\text{H}_2\text{O}$ , we prepared  $\text{Cu}_1\text{HPW}_{12}\text{O}_{40}$  and  $\text{Cu}_{0.5}\text{H}_2\text{PW}_{12}\text{O}_{40}$ . The catalyst mass was dried at 120 °C for 12 h in an oven and finally calcined at 300 °C for 2 h. The materials are further termed as  $\text{Cu}_x\text{H}_{3-2x}\text{PW}_{12}\text{O}_{40}$  ( $x=0.5-1.5$ ).

A series of catalysts having different Cu/HPA loading 10–60 wt% were synthesized by impregnating 2 g of MCM-41 with an aqueous solution of Cu/HPA under constant stirring followed by heating till complete evaporation of water takes place (4 h). Then the sample was dried in an oven at 110 °C for 24 h and calcined at 500 °C. The catalysts are herein after referred to as  $y\text{Cu}_x\text{H}_{3-2x}\text{PW}_{12}\text{O}_{40}/\text{MCM-41}$  ( $y=10-60$  wt%).

#### 3.4.2 Characterization

##### X-Ray Diffraction

The PXRD patterns of  $\text{H}_3\text{PW}_{12}\text{O}_{40}/\text{MCM-41}$  and  $50\text{Cu}_{1.5}\text{PW}_{12}\text{O}_{40}$ -promoted MCM-41 samples are shown in Fig. 3.5. It can be observed that both the materials exhibit a strong peak at  $2\theta=2.2^\circ$  due to (100) plane. Also, small peaks due to higher order (110), (200), and (210) plane reflections within  $5^\circ$  indicate the formation of well-ordered mesoporous materials. Thus, the mesoporosity remains intact after the modification of the silica network with  $\text{Cu}_x\text{H}_{3-2x}\text{PW}_{12}\text{O}_{40}$ . There is a little bit reduction and broadening of the (100) peak of  $\text{H}_3\text{PW}_{12}\text{O}_{40}/\text{MCM-41}$  after modification of  $\text{Cu}_{1.5}\text{PW}_{12}\text{O}_{40}$  indicating a slight disturbance in hexagonal symmetry [26].



**Fig. 3.5** Low angle ( $0\text{--}10^\circ$ ) XRD patterns of MCM-41 (a), HPA/MCM-41 (b),  $\text{Cu}_{1.5}\text{PA/MCM-41}$  (c)

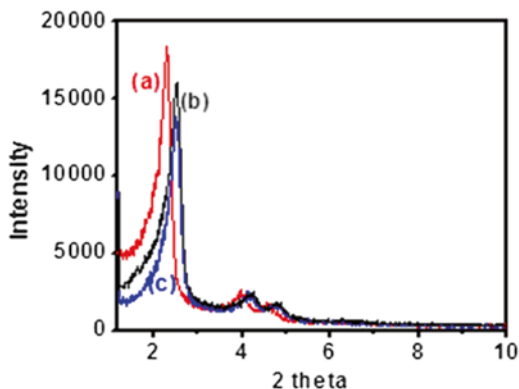
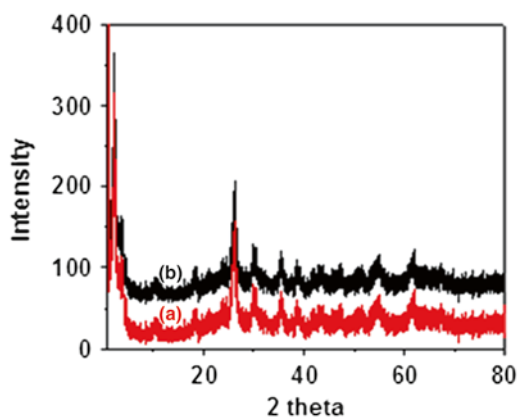


**Fig. 3.6** Wide angle ( $20\text{--}80^\circ$ ) XRD patterns of HPA/MCM-41 (a),  $\text{Cu}_{1.5}\text{PA/MCM-41}$  (b)

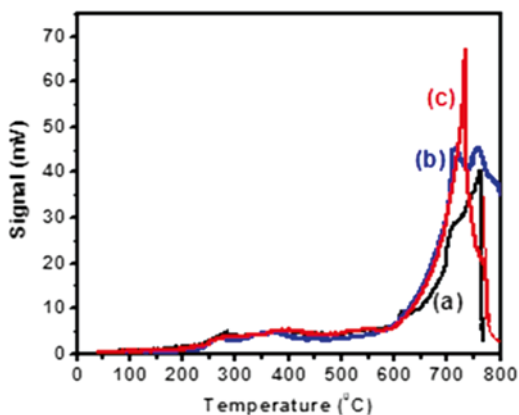


The characteristic peaks for HPA [27] are observed in both cases (Fig. 3.6), which indicated that the structure of HPA remains intact after metal modification.

### Temperature-Programmed Reduction

The temperature-programmed reduction profiles of the 50 wt% Cu-/HPA-modified MCM-41 are shown in Fig. 3.7. All the samples show reduction peaks in mainly two regions: one is around  $250\text{--}400^\circ\text{C}$  and another is  $650\text{--}800^\circ\text{C}$ . The first peak corresponds to reduction of  $\text{Cu}^{+2}$  to Cu metal. Reduction may take place in one step ( $\text{Cu}^{+2} \rightarrow \text{Cu}$ ) or in two subsequent steps ( $\text{Cu}^{+2} \rightarrow \text{Cu}^{+1} \rightarrow \text{Cu}$ ). The high-temperature reduction peak corresponds to reduction of CuHPA species adsorbed on the MCM-41 support. As a result of their high dispersion, these species interacting with the support are more easily reducible than the species of the bulk CuHPA. The peak intensity increases with increase in Cu content in the sample.

**Fig. 3.7** TPR spectra of  $\text{Cu}_{0.5}\text{H}_2\text{PA/MCM-41}$  (a),  $\text{Cu}_1\text{HPA/MCM-41}$  (b) and  $\text{Cu}_{1.5}\text{PA/MCM-41}$  (c)



### Transmission Electron Microscopy (TEM)

To study the surface topography and to assess the surface dispersion of the active components over the MCM-41 substrate, TEM investigation was performed on  $50\text{Cu}_{1.5}\text{PA/MCM-41}$  and the images are shown in Fig. 3.8. It has been found that the catalysts are well-ordered spherical particles. The particles are uniformly distributed over the support surface. TEM images of the mesoporous molecular sieves are characteristics for the mesoporous materials with hexagonal channel array, showing high quality in organization of channels of these catalysts. From the figure it is confirmed that the particles are spherical in nature. The metal particles are well dispersed throughout the silica framework, which is clearly seen in the figure. The particle size can be confirmed from the TEM images. The average particle size is calculated to be 100 nm.

### 3.4.3 Catalytic Evaluation Toward Heck Vinylation

Phenyl iodide (1 mmol), water (2 ml), and the catalyst (0.02 g) were taken in a round-bottom flask. The reaction mixture was stirred at 100 °C followed by the addition of acrylic acid (2 mmol) and  $\text{K}_2\text{CO}_3$  (1.5 mmol). After 8 h, the solution was allowed to cool down and filtered. The filtrate was analyzed by off-line GC and the solid residue was subjected to  $^1\text{H NMR}$ . The conversion was determined from the amount of phenyl iodide consumed in the reaction and is shown in Scheme 3.2. Leaching experiments for Cu metal were performed for each catalyst by using AAS analysis of the filtrates.

Two types of mechanisms are suggested for the Heck vinylation reaction. One is through the neutral pathway and another is the cationic pathway [10]. Yang et al. [28] suggested the mechanism for Heck vinylation using silica-supported poly- $\gamma$ -aminopropylsilane transition metal ( $\text{Ni}^{+2}$ ,  $\text{Cu}^{+2}$ ,  $\text{Co}^{+2}$ ) complexes similar to that of homogeneous catalyst for Heck reaction. In the case of homogeneous Pd catalyst, the Pd (IV) is reduced to Pd (II) during the reaction procedure.

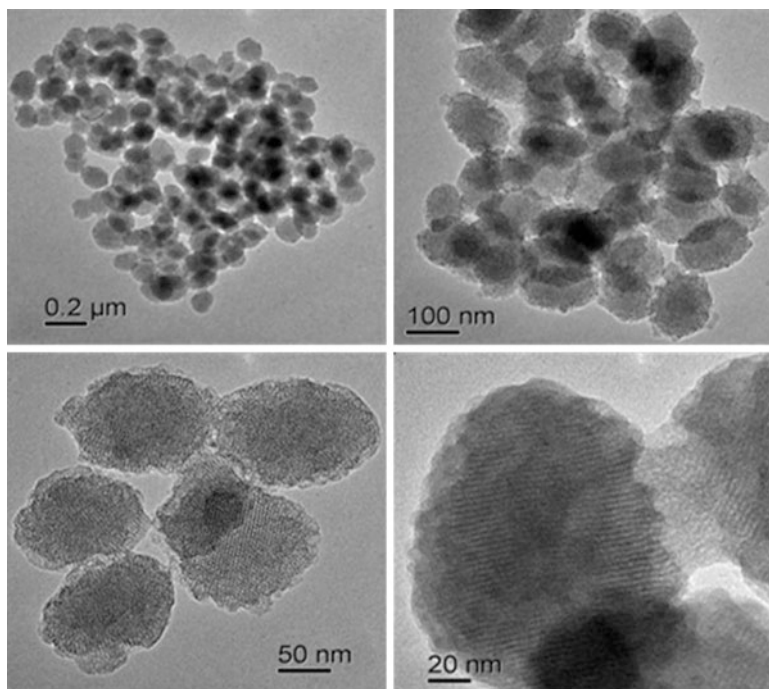
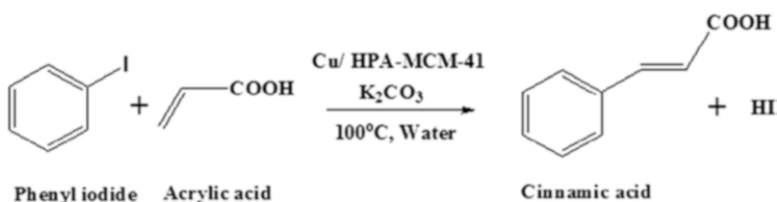


**Fig. 3.8** TEM images of 50Cu<sub>1.5</sub>PA/MCM-41

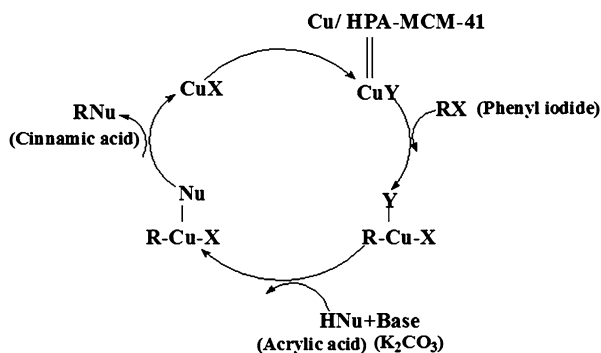


**Scheme 3.2** Schematic presentation of Heck vinylation reaction

Similarly we can assume the reaction will proceed by the reduction of supported Cu<sup>+2</sup> to the active Cu metal in case of CuHPA/MCM-41 (Scheme 3.3). First of all there is oxidative addition of phenyl iodide to CuHPA/MCM-41. With subsequent addition of HNu (acrylic acid) and base (K<sub>2</sub>CO<sub>3</sub>), there is reductive elimination of product (cinnamic acid) and the catalyst can be regenerated in subsequent steps.

Parent MCM-41 is less active toward Heck vinylation reaction and gave only 5 % conversion. In order to investigate the effect of Cu content, Cu<sub>0.5</sub>H<sub>2</sub>PW<sub>12</sub>O<sub>40</sub>, Cu<sub>1</sub>H<sub>1</sub>PW<sub>12</sub>O<sub>40</sub>, and Cu<sub>1.5</sub>PW<sub>12</sub>O<sub>40</sub> catalysts were used in Heck vinylation. From the experimental results we can confirm that the percentage of phenyl iodide conversion

**Scheme 3.3** Proposed mechanism for Heck vinylation reaction using Cu/HPA-MCM-41 as catalysts



increased from 88 to 98 % with increase in Cu content from 0.5 to 1.5 mol. Also the effect of CuHPA loadings was studied by using 10–60 wt% CuHPA/MCM-41 catalysts in Heck vinylation. Among the catalysts with different CuHPA loadings, the 50 wt% Cu<sub>1.5</sub>PW<sub>12</sub>O<sub>40</sub>/MCM-41 catalyst gave the highest conversion (98 %). With further increase in CuHPA loadings, there may be possibility of formation polylayer of material on the support surface. So the catalytic conversion decreased in a small extent (94 %) in case of 60Cu<sub>1.5</sub>PW<sub>12</sub>O<sub>40</sub>/MCM-41 and the materials are characterized by different technique.

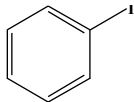
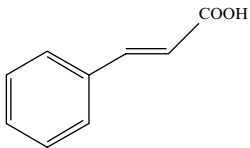
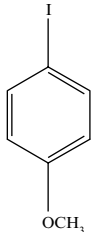
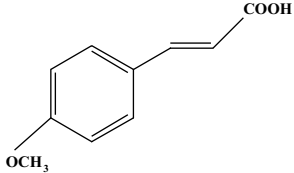
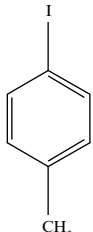
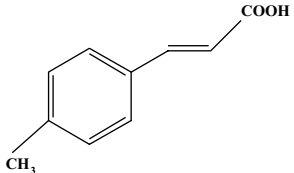
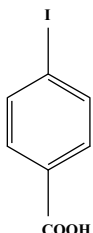
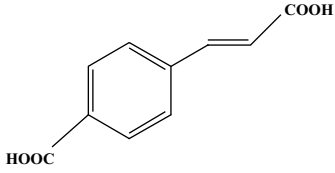
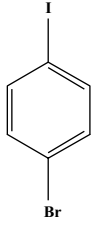
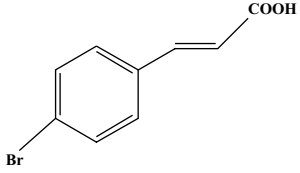
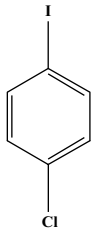
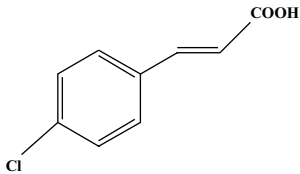
### 3.4.4 Influence of Various Substrates

Various aryl halides are tested toward Heck vinylation using acrylic acid as the olefin (Table 3.3). Electron-donating groups at the para position on the phenyl substrate enhanced the percentage of conversion, whereas electron-withdrawing groups decreased it. Electron-rich phenyl iodide is more appreciable to form complex with Cu (II) and attack the double bond of acrylic acid to form the product.

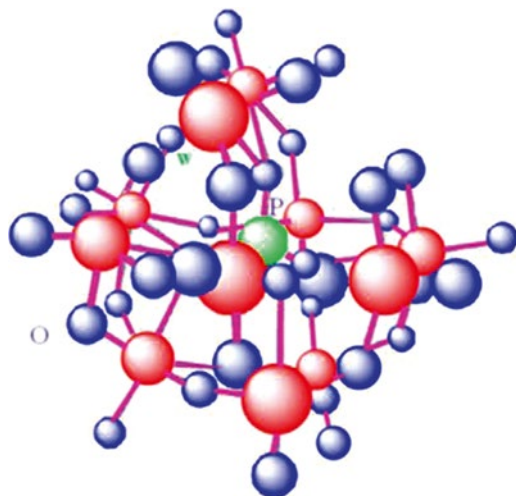
### 3.5 Fe-Modified Lacunary Phosphotungstate-Supported MCM-41 as an Excellent Catalyst for Acid-Catalyzed as well as Oxidation Reaction

The most investigated Keggin-type heteropoly acids are represented by the general formula  $[X^{n+}M_{12}O_{40}]^{(8-n)-}$ . Removal of one or two MO units from the fully occupied polyoxometalates  $[XM_{12}O_{40}]^{n-}$  gives rise to mono-lacunary  $[XM^{VI}_{11}O_{39}]^{(n+4)-}$  and di-lacunary  $[XM^{VI}_{10}O_{36}]^{(n+5)-}$  polyoxometalates, respectively.

**Table 3.3** Effect of substrates on the conversion of aryl halide

Substrate	Product	Conversion (%)
		98
		100
		100
		87
		72
		69

Aryl iodide=1 mmol, acrylic acid=2 mmol,  $K_2CO_3$ =1.5 mmol, water=2 ml, catalyst=0.02 g, temperature=100 °C, time=8 h



(Mono-lacunary)

Lacunary and di-lacunary polyoxometalates are gaining more importance because of their unique structural properties. It is well known that when the lacunary of Keggin anions  $[XW_{11}O_{39}]^{(n+4)-}$  is substituted by other transition metal cations, it gives rise to transition metal-modified lacunary heteropoly compounds having the general formula  $[XW_{11}O_{39}M]^{n-}$  (where M = first row transition metal). These species have recently attracted considerable attention [29], because of their thermal and chemical stability and the range of possibilities for their modification of electrocatalytic property without affecting the primary Keggin structure [30].

Recently, Patel et al. reported the detailed synthesis and characterization of Keggin-type manganese (II)-substituted phosphotungstate and its activity toward liquid phase oxidation of styrene [29]. Various works have already been carried out on Fe metal-substituted heteropoly acids. Mizuno et al. [31] reported synthesis of Fe, Ni-substituted Keggin-type heteropoly anion and evaluated its catalytic activity toward oxidation reaction. Nagai et al. reported iron in the Keggin anion of heteropoly acid catalysts for selective oxidation of isobutene [32]. But so far there is no literature available on the catalytic aspects of supported Cs salt of iron-substituted lacunary anions.

Many a study was already carried out on oxidation of *trans*-stilbene as well as bromination of phenol using various catalysts. Maurya and Amit Kumar [33] reported oxidation of *trans*-stilbene. But the inherent disadvantages associated were higher temperature and longer reaction time. Our group [34] reported bromination of phenol over heteropoly acid (HPA)-impregnated zirconium phosphate (ZrP), with 86 % conversion. But the most enchanting part of the present study is that this single catalyst is showing its superlative catalytic activity toward both the reactions.

We have investigated the use of various LFeW/MCM-41 as catalysts in the acid-catalyzed bromination of phenol as well as in the oxidation of *trans*-stilbene. The bromination of phenol was carried out in acetic acid medium with KBr and hydrogen peroxide at room temperature.

- (a) Synthesis of sodium salt of iron-substituted lacunary phosphotungstate ( $\text{Na}_5\text{FePW}_{11}\text{O}_{39}$ )

The sodium salt of lacunary heteropoly compound modified with iron ion was prepared by the alkalization of a solution of dodecatungstophosphoric acid with an aqueous solution of  $\text{NaHCO}_3$ . First  $\text{H}_3\text{PW}_{12}\text{O}_{40}\cdot n\text{H}_2\text{O}$  (2.88 g) was dissolved in water (10 ml) and the pH of the solution was adjusted to 4.8 using  $\text{NaHCO}_3$  solution. This resulted in the formation of lacunary heteropoly anion  $[\text{PW}_{11}\text{O}_{39}]^{7-}$ . The solution having pH 4.8 was heated to 90 °C with constant stirring. A solution of  $\text{FeCl}_2$  (0.197 g, 1 mmol) in water (10 ml) was added to this hot solution. The  $\text{Na}_5\text{FePW}_{11}\text{O}_{39}$  was obtained by solvent evaporation and recrystallization from water, followed by subsequent drying at 110 °C for 12 h.

- (b) Synthesis of Cs salt of iron-substituted lacunary phosphotungstate supported onto MCM-41 ( $x$  LFeW/MCM-41)

A series of catalysts having different loading of Cs salt of Fe-modified lacunary phosphotungstate (30–60 wt%)-promoted MCM-41 were synthesized by incipient weight impregnation method by adopting the following procedure.

MCM-41 was first impregnated with aqueous solution of the  $\text{Cs}^+$  precursor ( $\text{Cs}_2\text{CO}_3$ ), dried at 110 °C for 12 h. Following this, an aqueous solution of  $\text{Na}_5\text{FePW}_{11}\text{O}_{39}$  was impregnated, dried at 110 °C for 12 h, and calcined at 200 °C for 3 h. The catalysts are designated as  $x$  LFeW/MCM-41 ( $x = 30\text{--}60$  wt%).

- (c) Synthesis of cesium salt of iron-substituted lacunary phosphotungstate (LFeW) and Cs salt of lacunary phosphotungstate (LW)

The preparation procedure for LFeW was same as described in the section for the preparation of  $\text{Na}_5\text{FePW}_{11}\text{O}_{39}$  up to the addition of  $\text{FeCl}_2$ . After which a saturated solution of the  $\text{Cs}_2\text{CO}_3$  was added to the hot filtrate and the resulting mixture was allowed to stand overnight at room temperature. The mixture was filtered and the residue was dried at 110 °C for 12 h, which resulted in LFeW. The filtrate was used for the estimation of W and Fe, in order to see the loss during synthesis.

### 3.5.1 Characterization

#### Surface Area and Pore Size Distribution

The nitrogen adsorption–desorption isotherms for MCM-41 and 50 LFeW/MCM-41 are shown in Fig. 3.9.  $\text{N}_2$  sorption resulted typical type IV isotherm which is defined by Brunauer et al. [35]. It is observed that there are three different well-defined stages in the isotherm of MCM-41. The initial increase in nitrogen uptake at low  $P/P_0$  may be due to monolayer adsorption on the pore walls; a sharp steep increase at intermediate  $P/P_0$  indicates the capillary condensation in the mesopores and a plateau portion at higher  $P/P_0$  is associated with multilayer adsorption on the external surface of the materials [35].

Parent MCM-41 sample exhibits  $\text{N}_2$  uptake at a relative pressure of 0.32 which corresponds to the pre-condensation loop. The isotherm shows a H4-type hysteresis

**Fig. 3.9** N<sub>2</sub> ads-des isotherm of MCM-41 (a) and 50 LFeW/MCM-41 (b)

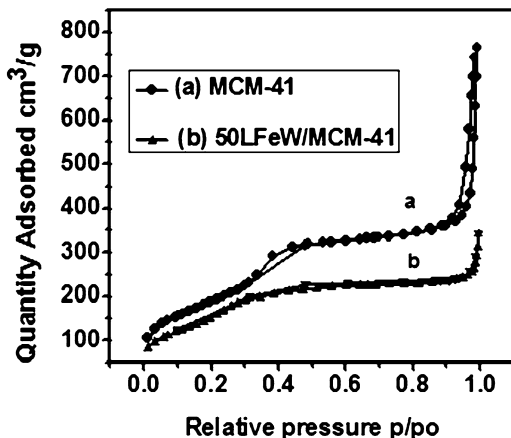
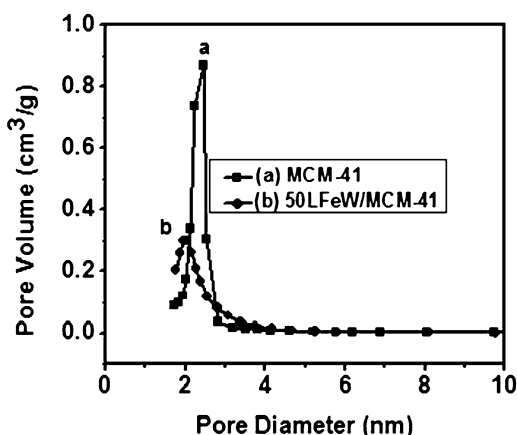


**Fig. 3.10** Pore size distribution curve of MCM-41 (a) and 50 LFeW/MCM-41 (b)

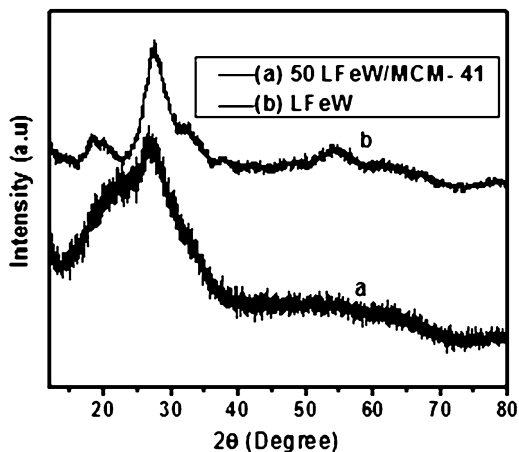


loop (according to IUPAC nomenclature) with well-developed step in the relative pressure range  $\approx 0.9$ . The incorporation of LFeW in the MCM-41 framework is found to lower the  $P/P_0$  value for capillary condensation step, indicating the shift in pore size to lower value due to incorporation of lacunary acid. The pore diameter is found to decrease with increasing loading of LFeW content over the MCM-41 surface (Fig. 3.10).

The textural properties such as BET surface area, pore diameter, and pore volume derived from the N<sub>2</sub> adsorption-desorption measurements. The parent MCM-41 has a surface area of 1,250 m<sup>2</sup>/g. But there is a gradual decrease in the value with increasing LFeW content in MCM-41. This may be due to the fact that increasing loading may result in the formation of polylayer on the pores of the silica surface. Pore size and pore volume exhibit similar trend as that of surface area. There is a gradual decrease in the values with increasing LFeW content on MCM-41 samples.



**Fig. 3.11** Wide angle (10–80°) XRD patterns of (a) 50 LFeW/MCM-41 and (b) LFeW



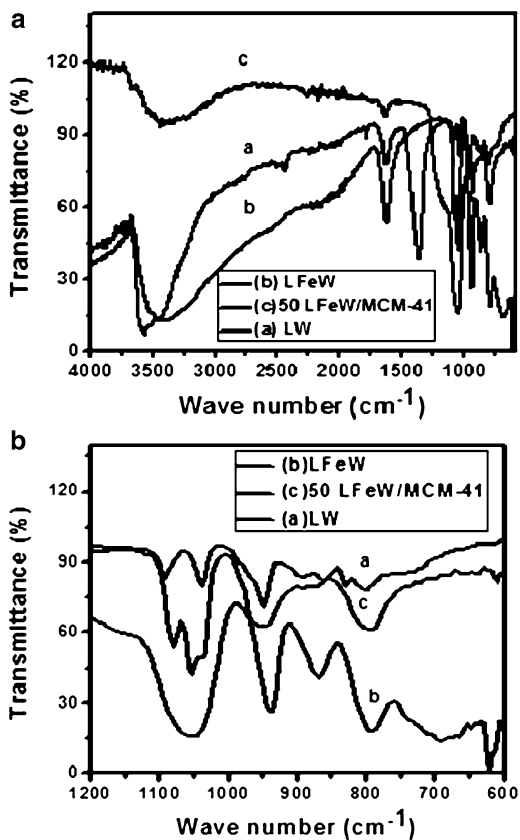
### X-Ray Powder Diffraction Studies

The wide angle XRD of LFeW and LFeW/MCM-41 is shown in Fig. 3.11. The XRD pattern of LFeW shows that it is crystalline in nature. But in the case of 50 LFeW/MCM-41 sample, the XRD pattern shows a broad peak showing no characteristic peaks of LFeW, indicating a very high dispersion of LFeW in a noncrystalline form on the surface of MCM-41.

### FTIR Studies

The FTIR spectra of various samples are shown in Fig. 3.12. In the case of LFeW/MCM-41, the broad band around  $3,500\text{ cm}^{-1}$  may be attributed to surface silanols and adsorbed water molecules, while deformational vibrations of adsorbed molecules cause the absorption bands at  $1,623\text{--}1,640\text{ cm}^{-1}$  [36]. The spectrum of the Keggin anion  $[\text{PW}_{12}\text{O}_{40}]^{3-}$  shows prominent bands at  $1,080, 985, 890,$  and  $800\text{ cm}^{-1}$  which are characteristic of Keggin structure and are assigned to  $\nu_{(\text{P}-\text{O})}$ ,  $\nu_{(\text{W}=\text{O})}$ , corner-sharing  $\nu_{(\text{W}-\text{O}-\text{W})}$ , and edge-sharing  $\nu_{(\text{W}-\text{O}-\text{W})}$ , respectively [37]. In the case of LW, the  $1,080\text{ cm}^{-1}$  band has been split into two components ( $1,084\text{--}1,044\text{ cm}^{-1}$ ), due to the symmetry decrease of the  $\text{PO}_4$  tetrahedron. The other bands found are  $953\text{ (}\nu_{\text{as}(\text{W}-\text{O}_d\text{))}$ ,  $860\text{ (}\nu_{\text{as}(\text{W}-\text{O}_b\text{-W))}$ ,  $809,$  and  $742\text{ cm}^{-1}$  ( $\nu_{\text{as}(\text{W}-\text{O}_c\text{-W})}$ ) and differ from those of  $[\text{PW}_{12}\text{O}_{40}]^{3-}$  [37]. The spectra for LFeW showed characteristic splitting for the P–O bond frequency at  $1,074$  and  $1,052\text{ cm}^{-1}$ , which faced a slight shifting toward lower frequency compared to bulk lacunary unit. This clearly indicated that Fe was introduced into the octahedral lacuna. The slight shifting of bands in FTIR spectra of LFeW sample compared to bulk LW may be due to formation of pseudosymmetric environment that resulted from the replacement of a W atom with a Fe atom. It can be observed that 50 LFeW/MCM-41 sample has similar vibration bands to those of the corresponding

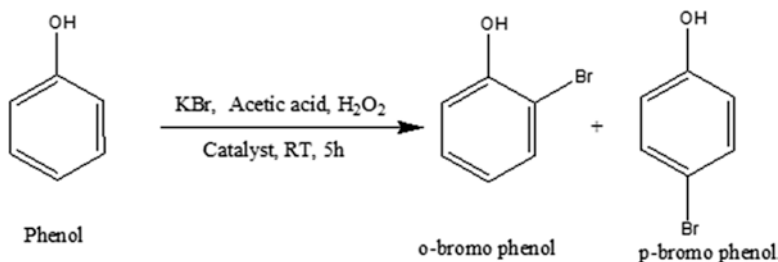
**Fig. 3.12** FTIR spectra of LW (a), LFeW (b) and 50 LFeW/MCM-41 (c)



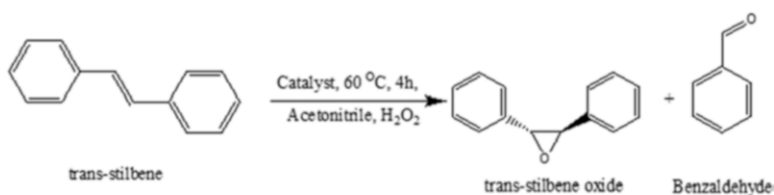
pure LFeW, which suggests that the LFeW structures remained intact regardless of their functionality. The shifting in the positions of the IR absorption peaks is due to both hydrogen bonding and chemical interactions that exist between the surface of LFeW and the MCM-41.

### 3.5.2 Catalytic Activity Toward Bromination of Phenol and Oxidation of *trans*-Stilbene

Bromination of phenol was carried out in a 50 ml two-necked round-bottom flask, charged with 0.2 g catalyst, phenol (2 mmol) in acetic acid (4 ml), and KBr (2.2 mmol). Then 30 %  $\text{H}_2\text{O}_2$  (2.2 mmol) was added dropwise to the reaction mixture and the contents in the flask was stirred continuously at room temperature for 5 h [38]. After 5 h of the reaction, the catalyst was filtered and the solid was washed with ether. The combined filtrates were washed with saturated sodium bicarbonate solution and then shaken with ether in a separating funnel. The organic extract was dried over anhydrous sodium sulfate. The products were analyzed by GC, through capillary column (Scheme 3.4).



**Scheme 3.4** Schematic representation of bromination of phenol



**Scheme 3.5** Schematic representation of *trans*-stilbene oxidation

The oxidation of *trans*-stilbene was carried out in a 50 ml two-necked round-bottom flask, provided with a mercury thermometer for measuring the reaction temperature and a reflux condenser. The reaction mixture containing 0.015 g catalyst, 1.82 g *trans*-stilbene (10 mmol) and 30 %  $\text{H}_2\text{O}_2$  (20 mmol), 20 ml of acetonitrile was heated at 60 °C for 4 h in an oil bath with stirring. The reaction products were analyzed by gas chromatograph using capillary column (ZB MAX) (Scheme 3.5).

Fe metal-modified Keggin-type lacunary phosphotungstate-supported mesoporous silica acts as an excellent catalyst for acid-catalyzed bromination of phenol as well as oxidation reaction of *trans*-stilbene. The 50 wt%  $\text{Cs}_5$  [ $\text{PFeW}_{11}\text{O}_{39}$ ]/MCM-41 showed remarkable catalytic performance, obtaining mono bromophenol having 95 % conversion with 99 % selectivity and *trans*-stilbene oxide having 52 % conversion with 99 % selectivity. The materials are characterized by different techniques.

### 3.6 Cs Salt of Pd Substituted Lacunary Phosphotungstate-Supported MCM-41 Toward Hydrogenation of p-Nitrophenol to p-Aminophenol

Considering enormous interest in palladium chemistry, it must be realized that homogeneous palladium catalysis has gained great success in Suzuki cross-coupling as well as other coupling reactions for the formation of C–C bonds [39]. To address the disadvantages associated with the homogeneous catalysis, one of the effective strategies is to support palladium on various inorganic supports including mesoporous

silica, mesoporous alumina, mesoporous tin, and mesoporous carbon [40–44] and polymers [45, 46]. Palladium constitutes a very promising catalyst toward hydrogenation reactions [47].

Various methods have been reported earlier to synthesize *p*-aminophenol, such as multistep iron–acid reduction of *p*-nitrochlorobenzene or *p*-nitrophenol [48], catalytic hydrogenation of nitrobenzene [49], and electrochemical synthesizing method. However, to meet the growing commercial demand of *p*-aminophenol, the direct catalytic hydrogenation of *p*-nitrophenol is presently becoming important. So in this study we tried to explore the reducing ability of Keggin-type Cs salt of palladium metal-substituted mono-lacunary phosphotungstate-supported mesoporous silica (Cs<sub>5</sub> [PPdW<sub>11</sub>O<sub>39</sub>]/MCM-41) toward catalytic hydrogenation of *p*-nitrophenol to *p*-aminophenol. The catalyst showed eye-catching activity toward the desired reaction.

- (a) Synthesis of sodium salt of palladium substituted lacunary phosphotungstate (Na<sub>5</sub>PdPW<sub>11</sub>O<sub>39</sub>)

The sodium salt of lacunary heteropoly compound modified with palladium ion was prepared by the alkalization of a solution of dodecatungstophosphoric acid with an aqueous solution of NaHCO<sub>3</sub>. First H<sub>3</sub>PW<sub>12</sub>O<sub>40</sub>·*n*H<sub>2</sub>O (2.88 g) was dissolved in water (10 ml) and the pH of the solution was adjusted to 4.8 using NaHCO<sub>3</sub> solution. This resulted in the formation of lacunary heteropoly anion [PW<sub>11</sub>O<sub>39</sub>]<sup>7-</sup>. The solution having pH 4.8 was heated to 90 °C with constant stirring. A solution of PdCl<sub>2</sub> (0.177 g, 1 mmol) in water (10 ml) was added to this hot solution. The Na<sub>5</sub>PdPW<sub>11</sub>O<sub>39</sub> was obtained by solvent evaporation and recrystallization from water, followed by subsequent drying at 110 °C for 12 h.

- (b) Synthesis of Cs salt of palladium-substituted lacunary phosphotungstate supported onto MCM-41 (*x* LPdW/MCM-41)

MCM-41 was first impregnated with aqueous solution of the Cs<sup>+</sup> precursor (Cs<sub>2</sub>CO<sub>3</sub>), dried at 110 °C for 12 h. Following this, a methanolic solution of Na<sub>5</sub>PdPW<sub>11</sub>O<sub>39</sub> was impregnated, dried at 110 °C for 12 h, and calcined at 200. The catalysts are designated as *x* LPdW/MCM-41 (*x* = 30–60 wt%). The materials are characterized by different technique.

### 3.6.1 Characterization

#### X-Ray Powder Diffraction Studies

The PXRD patterns of MCM-41 and 50 LPdW/MCM-41 samples are shown in Fig. 3.13. It can be observed that both materials exhibit a strong peak at about  $2\theta = 2.2^\circ$  due to reflection at (100) plane. A little bit reduction and broadening of the (100) peak of 50 LPdW/MCM-41 which can be seen with a slight shift toward a higher  $2\theta$  indicates a slight disturbance in its hexagonal symmetry. Also small peaks

**Fig. 3.13** Low angle (0–10°) XRD patterns of MCM-41 and 50 LPdW/MCM-41

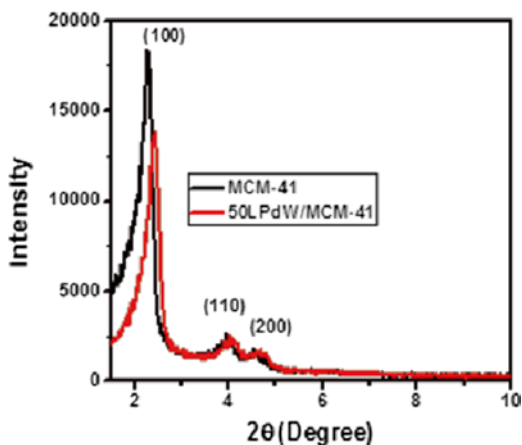
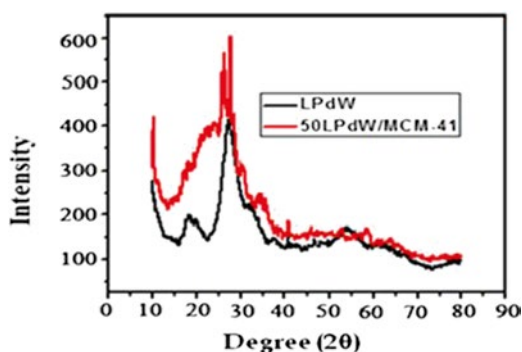


**Fig. 3.14** PXRD of LPdW and 50 LPdW/MCM-41



due to higher order reflections at (110), (200), and (210) planes within 5° indicate that both the materials possess well-ordered mesoporosity [50].

The wide angle PXRD of LPdW and 50LPdW/MCM-41 is shown in Fig. 3.14. The XRD pattern of palladium metal has major diffraction peaks at  $2\theta = 40.1^\circ$  (111) and  $46.7^\circ$  (200), which is in agreement with the reported literature [51]. The characteristic peaks for LPdW are observed in both cases, which indicate that the structure of LPdW remains intact after metal modification.

### $^{31}\text{P}$ MAS NMR Spectrum Studies

The  $^{31}\text{P}$  MAS NMR spectrum for 50LPdW/MCM-41 catalyst is shown in Fig. 3.15. The spectra show two peaks, the main peak at  $-15.4$  ppm and small peaks at  $-13.5$  ppm. From the literature [52], the spectra of LPdW shows two peaks, the major peak at  $-15.17$  ppm (95 %) attributable to  $[\text{PPdW}_{11}\text{O}_{39}]^{5-}$  and a small peak at  $-13.32$  ppm (5 %) attributable to an impurity of the starting material,  $[\text{PW}_{11}\text{O}_{39}]^{7-}$ . The 50 LPdW/MCM-41 catalysts with high LPdW content exhibit a sharp resonance at  $-15.4$  ppm,

**Fig. 3.15**  $^{31}\text{P}$  MAS NMR spectra of 50 LPdW/MCM-41

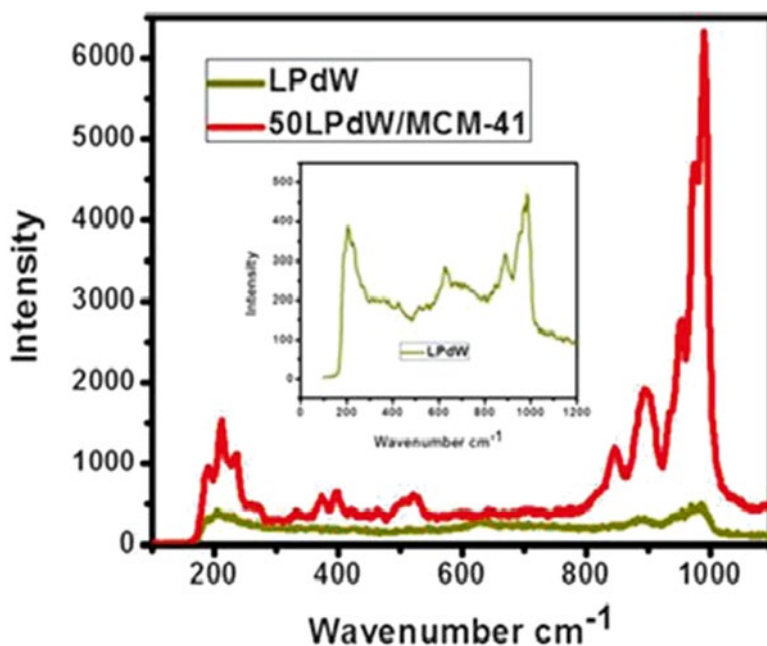
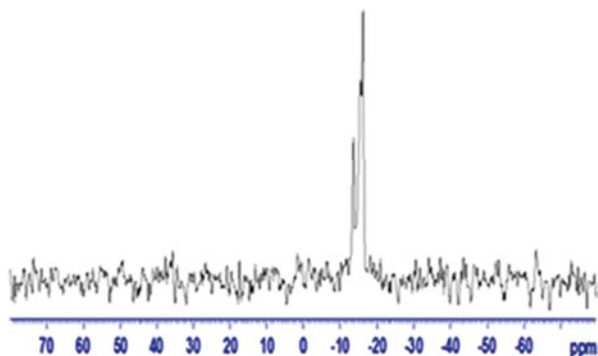


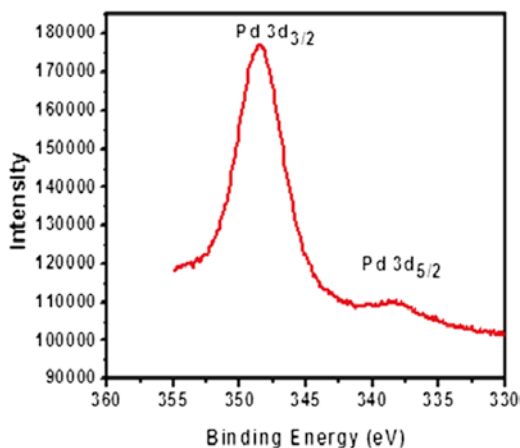
**Fig. 3.16** Raman spectroscopy of LPdW and 50LPdW/MCM-41

which is close to that of bulk LPdW. This indicates unambiguously that the Keggin structure is retained even after LPdW is loaded on MCM-41, and it is slightly shifted toward right due to chemical interaction, hydrogen bonding, and covalent bonding between support and LPdW.

### Raman Spectroscopy

Figure 3.16 shows the Raman scattering spectroscopy of LPdW and 50 LPdW/MCM-41. The bulk LPdW gives peaks at 984, 888, 847, and 799  $\text{cm}^{-1}$  which are

**Fig. 3.17** XPS spectrum of Pd  $3d_{3/2}$  and Pd  $3d_{5/2}$  of 50 LPdW/MCM-41



attributed to the stretching vibrations of P–O, W–Ob–W, W–Oc–W, and W–Ot bonds of metal-modified mono-lacunary Keggin unit, respectively. The 50 LPdW/MCM-41 sample shows all the above-described bands of LPdW, but the intensities of the bands are low and slightly shifted toward higher wave number due to strong interactions between MCM-41 support and lacunary Keggin unit [53].

### XPS Spectrum Studies

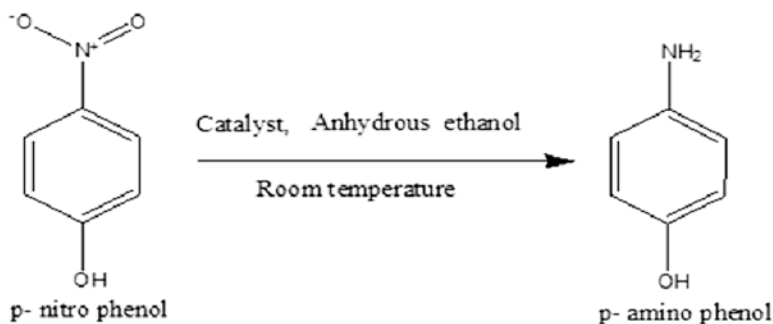
The incorporation of Pd ions into lacunary phosphotungstate, its oxidation states, and its interaction with the support were confirmed from XPS measurements. The Pd 3d XPS spectrum of 50 LPdW/MCM-41 sample are shown in Fig. 3.17.

From this figure two distinct palladium peaks were observed at binding energies 338.7 and 347.9 eV. The binding energy of about 337.9 eV for the Pd 3d 5/2 peak is reported in the literature [53]. However, shifting of 3d 5/2 peak toward a higher binding energy suggests the interaction of Pd (II) with the support surface [53].

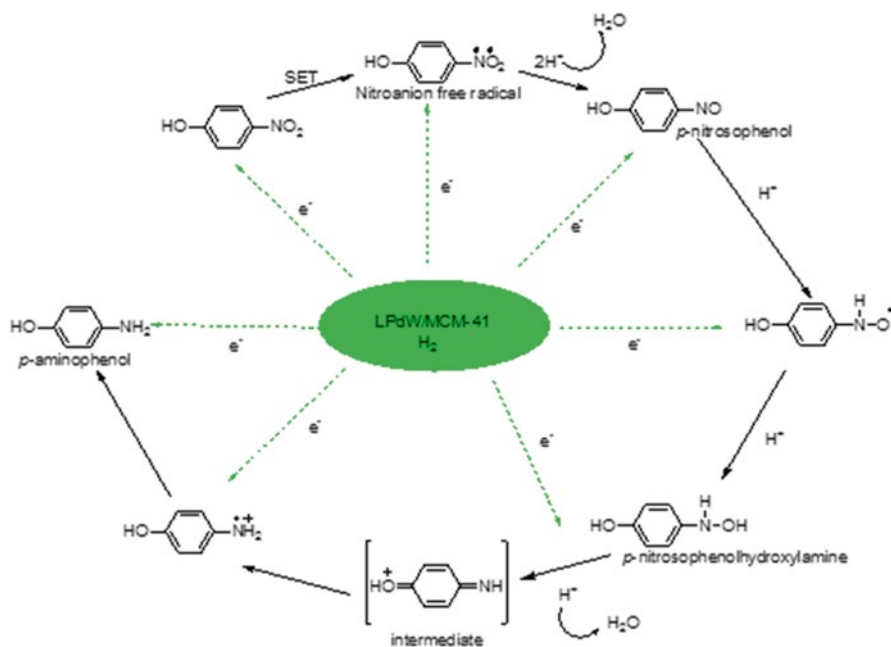
### 3.6.2 Catalytic Activity Toward Hydrogenation of *p*-Nitrophenol to *p*-Aminophenol

The hydrogenation of *p*-nitrophenol was carried out in a two-necked round-bottom flask with a reflux condenser at atmospheric pressure, which was charged with 1.0 g of *p*-nitrophenol dissolved in 50 ml anhydrous ethanol and 0.05 g of catalyst. The flask was purged with nitrogen for 10 min. The reaction was started by vigorous stirring of the reaction mixture under H<sub>2</sub> gas-flow (10 ml min<sup>-1</sup>) at room temperature for 1 h. The reaction products were analyzed by off-line gas chromatography (Scheme 3.6).

A green and effective method is reported for the hydrogenation of *p*-nitrophenol to *p*-aminophenol using a Cs salt of Pd-substituted Keggin-type mono-lacunary



**Scheme 3.6** Schematic representation of *hydrogenation of p-nitrophenol to p-aminophenol*



**Scheme 3.7** Mechanism of hydrogenation of *p*-nitrophenol to *p*-aminophenol

phosphotungstate-supported mesoporous silica (LPdW/MCM-41). This economical and environmentally friendly method carried out at room temperature gives 99 % conversion and 100 % selectivity.

As shown in Scheme 3.7, a mechanism is proposed for this reaction. The key step in this mechanism involves the single electron transfer (SET) to form a nitro anion free radical. The subsequent step involves the electron transfer and also hydrogen ion transform to form an intermediate. The intermediate then gets converted to *p*-aminophenol.



## 4 Conclusions

We have successfully synthesized Cs salt of phosphotungstic acid, Cu salt of phosphotungstic acid, Fe-modified lacunary phosphotungstate, and Cs salt of Pd-substituted lacunary phosphotungstate supported on MCM-41 and unambiguously characterized by XRD, UV-vis DRS, FTIR, BET surface area, acid sites by ammonia TPD, and morphology by SEM. The catalytic activity of the transition metal salts of polyoxometalate-promoted MCM-41 was evaluated for various organic transition reactions. Among the catalysts with different Cs-PTA loadings, the 50 wt% Cs-PTA/MCM-41 catalyst gave the highest conversion (98 %) toward acylation of anisole with acetic anhydride. 50 wt%  $\text{Cu}_{1.5}\text{PW}_{12}\text{O}_{40}$ /MCM-41 catalyst gave the highest conversion (98 %) of phenyl iodide to cinnamic acid (Heck vinylation reaction). The 50 wt%  $\text{Cs}_5[\text{PFeW}_{11}\text{O}_{39}]$ /MCM-41 showed remarkable catalytic performance, obtaining mono bromophenol having 95 % conversion with 99 % selectivity and *trans*-stilbene oxide having 52 % conversion with 99 % selectivity. Out of various wt% of the lacunary salt loadings, 50LPdW/MCM-41 was found to be an excellent catalyst toward hydrogenation of *p*-nitrophenol to *p*-aminophenol at room temperature. The catalyst could be reused several times without a significant degradation in catalytic activity. This suggests the commercial exploitation of this polyoxometalate-based heterogeneous catalyst for the synthesis of additional organic target molecules.

**Acknowledgments** The authors are thankful to Prof. B. K. Mishra, Director, IMMT (CSIR), Bhubaneswar, for his keen interest, encouragement, and kind permission to publish this work. Mr. Surjyakanta Rana is obliged to CSIR for a senior research fellowship. We are thankful to DST for the financial support.

## References

1. Tanabe K (1970) Solid acid and bases. Academic, Tokyo
2. Tanabe K, Holderich WF (1999) Appl Catal A 181:399
3. Mizuno N, Misono M (1994) J Mol Catal 86:319
4. Kozhevnikov IV (1987) Russ Chem Rev 56:811
5. Cavani F (1998) Catal Today 41:73
6. Misono M, Okuhara T (1993) CHEMTECH 23:23
7. Kozhevnikov IV, Matveev KI (1983) Appl Catal 5:135
8. Pizzio LR, Caceres CV, Blanco MN (1999) Appl Surf Sci 151:91
9. Kozhevnikov IV (1995) Catal Rev Sci Eng 37:311
10. Misono M (1987) Cat Rev Sci Eng 29:269
11. Moffat JB, Kasztelan S (1988) J Catal 109:206
12. Izumi Y, Ogawa M, Ohara WN, Urabe K (1992) Chem Lett 39:1987
13. Pizzio LR, Caceres CV, Blanco MN (1998) Appl Catal A 167:283
14. Pizzio LR, Vazquez PG, Caceres CV, Blanco MN (2003) Appl Catal A 256:125
15. Knifton JF, Edwards JC (1999) Appl Catal A 183:1
16. Rao PM, Wolfson A, Landau MV, Herskowitz M (2004) Catal Commun 5:327

17. Cardoso LAM, Alves W Jr, Gonzaga ARE, Aguiar LMG, Andrade HMC (2004) *J Mol Catal A Chem* 209:189
18. Kaur J, Kozhevnikov IV (2002) *Chem Commun* 21:2508
19. Sarsani VR, Lyon CJ, Hutchenson KW, Harmer MA, Subramaniam B (2007) *J Catal* 245:184
20. Kamala P, Pandurangan A (2008) *Catal Commun* 9:2231
21. Luque R, Campelo JM, Luna D, Marinas JM, Romero AA (2005) *Microporous Mesoporous Mater* 84:11
22. Staiti P, Freni S, Hocevar S (1999) *J Power Sources* 79:250
23. Okuhara T, Nishimura T, Watanabe H, Misono M (1999) *J Mol Catal* 74:247
24. (a) van de Water LGA, van der Waal JC, Jansen JC, Maschmeyer T (2004) *J Catal* 223:170; (b) El Berrichi Z, Cherif L, Orsen O, Fraissard J, Tessonnier JP, Vanhaecke E, Louis B, Ledoux MJ, Pham-Huu C (2006) *Appl Catal A Gen* 298:194; (c) Selvin R, Hsiu-Ling Hsu, Tze-Min Her (2008) *Catal Commun* 10:169; (d) Pei Chun Shih, Jung-Hui Wang, Chung-Yuan Moub (2004) *Catal Today* 93:365; (e) Shih PC, Wang JH, Mou CY (2004) *Catal Today* 365:93; (f) Yadav GD, Asthana NS, Kamble VS (2003) *J Catal* 217:88; (g) Parida KM, Mallick S, Pradhan GC, (2009) *J Mol Catal A Chem* 297:93
25. (a) Corma A, Martinez A, Martinez C, (1996) *J Catal* 164:422; (b) Pizzio LR, Blanco MN, (2003) *Appl Catal A Gen* 255:265; (c) Saemin Choi, Yong Wang, Zimin Nie, Jun Liu, Charles HF Peden (2000) *Catal Today* 55:117; (d) Yadav JS, Subba Reddy BV, Purnima KV, Nagaiah K, Lingaiah N (2008) *J Mol Catal A Chem* 285:36
26. Liu Y, Xu L, Xu B, Li Z, Jia L, Guo W (2009) *J Mol Catal A Chem* 297:86
27. Baeza B, Rodriguez J, Ruiz A, Ramos I (2007) *Appl Catal A* 333:281
28. Hu J, Wang Y, Chen L, Richards R, Yang W, Liu Z, Xu W (2006) *Microporous Mesoporous Mater* 93:158
29. Patel K, Shringarpure P, Patel A (2011) *Trans Met Chem* 36:171
30. Pope MT (1983) *Heteropoly and isopoly oxometalates*. Springer, Berlin
31. Mizuno N, To-oru Hirose, Tateishi M, Iwamoto M (1994) *J Mol Catal* 88:125
32. Knapp C, Ui T, Nagai K, Mizuno N (2001) *Catal Today* 71:111
33. Maurya MR, Amit Kumar (2006) *J Mol Catal A Chem* 250:190
34. Das DP, Parida KM (2006) *Appl Catal A Gen* 305:32
35. Brunauer S, Deming LS, Deming E, Teller E (1940) *J Am Chem Soc* 62:1723
36. Parida KM, Rath D (2004) *J Mol Catal A Chem* 258:381
37. Nowinska K, Waclaw A, Masierak W, Gutsze A (2004) *Catal Lett* 92:157
38. Narender N, Krishna Mohan KVV, Vinod Reddy R, Srinivasu P, Kulkarni SJ, Raghavan KV (2003) *J Mol Catal A Chem* 192:73
39. Miyaura N, Suzuki A (1995) *Chem Rev* 95:2457
40. Gruber M, Chouzier S, Koehler K, Djakovitch L (2004) *Appl Catal A Gen* 265:161
41. Jin M-J, Taher A, Kang H-J, Choi M, Ryoo R (2009) *Green Chem* 11:309
42. Choudary BM, Madhi S, Chowdari NS, Kantam ML, Sreedhar B (2002) *J Am Chem Soc* 124:14127
43. Jamwal N, Gupta M, Paul S (2008) *Green Chem* 10:999
44. Hagio H, Sugiura M, Kobayashi S (2006) *Org Lett* 8:375
45. Han W, Liu C, Jin Z (2008) *Adv Synth Catal* 350:501
46. Mori A, Miyakawa Y, Ohashi E, Haga T, Maegawa T, Sajiki H (2006) *Org Lett* 8:3279
47. Rode CV, Vaidya MJ, Jaganathan R, Chaudhari RV (2001) *Chem Eng Sci* 56:1299
48. Vaidya MJ, Kulkarni SM, Chaudhari RV (2003) *Org Process Res Dev* 7:202
49. Kruk M, Jaroniec M, Ji Man Kim, Ryoo R (1999) *Langmuir* 15:5279
50. Mehnert CP, Ying JY (1997) *Chem Commun* 2215
51. Kogan V, Aizenshtat Z, Neumann R (2002) *New J Chem* 26:272
52. Ali Abdalla ZE, Li B, Tufail A (2009) *Colloid Surf A Physicochem Eng Asp* 341:86
53. Yang H, Zhang G, Hong X, Zhu Y (2004) *J Mol Catal A: Chem* 210:143